STRIPLINE BEAM POSITION MONITORS WITH IMPROVED FREQUENCY RESPONSE AND THEIR COUPLING IMPEDANCES

Y. Shobuda, J-PARC Center, JAEA, Ibaraki, JAPAN,
Y. H. Chin, K. Takata, T. Toyama, KEK, Tsukuba, Ibaraki, JAPAN
K. G. Nakamura, Kyoto University, Kyoto, JAPAN

Abstract

In J-PARC MR, there is a concern that electron cloud instabilities may appear and limit the beam current at future higher power operations. For the case, we have developed a wider-band beam position monitor by deforming the electrode shapes. The modification of the electrode can be done without significant enhancement of the beam coupling impedance. For typical electrode shapes, we show the coupling impedances as well as the frequency responses of the electrodes.

INTRODUCTION

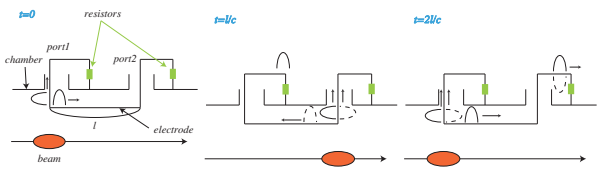

Figure 1: Flow chart of the induced pulses at a BPM.

Stripline beam position monitors (BPMs) are widely used for measurements of beam position signals in study of beam instabilities. The electrode is placed inside of the chamber. Figure 1 schematically shows the principle of the working of the BPMs.

Based on two-dimensional theory, the frequency response of the BPM is analytically given by the transfer function $F(\omega)$ as [1]

$$F(\omega) = i\omega \int_0^{\frac{2l}{c}} \frac{1}{2} k(\frac{ct}{2}) e^{-i\omega t} dt = \frac{i\omega}{c} \int_0^l k(z) e^{-i\frac{2\omega}{c}z} dz, \quad (1)$$

where i is imaginary unit, ω is angular frequency, $k(z)$ is the coupling function to the fields at point z, l is the electrode length and the velocity of the beam is approximated by the speed of light c.

For the electrode in a shape of rectangle, the transfer function is calculated as

$$F(\omega) = k_0 \frac{(1 - e^{-i\omega\frac{2l}{c}})}{2}, \quad (2)$$

by extracting the z-dependence from the coupling function $k(z) = k_0$. The distinctive feature of this function is that the absolute value has sharp notches with its interval: $f_n = nc/2l$, where n is integer (see the red lines in Fig.2).

The origin of these notches can be qualitatively understood as follows. As Fig.1 shows, when a beam arrives at the front-end of the electrode ($t = 0$), the beam excites two currents with opposite polarities. One current flows to the downstream with the beam, while the other does to the upstream side and enters the port1.

When the beam reaches the back-end of the electrode ($t = l/c$), new currents with opposite polarities (the dashed-pulse) are additionally excited there. The total signal to the port 2 is cancelled by superposing the currents (the solid and the dashed pulses at $t = l/c$).

When successive pulse trains come with their interval $2l/c$, the subsequent pulse (the solid pulse at $2l/c$) compensates the prior signal (the dashed pulse) crated by the predecessor pulse as in the figure at $t = 2l/c$. Finally, all beam-induced signals with the frequency : f_n cannot be detected at all outside the chamber.

THE IDEAL ELECTRODE SHAPE

To avoid the demerit of the rectangular electrode, no pair of image currents should be generated by the leaving pulse. It is enabled by narrowing the electrode toward downstream and carefully reclining the electrode to the chamber, to preserve the characteristic impedance Z_c of the electrode.

In 1970's Linnecar suggested an exponential electrode for better frequency characteristic [2]. When the coupling function $k(z)$ is given by

$$k(z) = k_0 e^{-\frac{az}{l}}, \quad (3)$$

the transfer function $F(\omega)$ is calculated as

$$F(\omega) = k_0 \frac{i\omega l(1 - e^{-a - i\frac{2\omega l}{c}})}{c(a + \frac{i2\omega l}{c})}, \quad (4)$$

where a is a positive dimensionless parameter defining the degree of the exponential tapering of the electrode. The blues line in the left figure of Fig.2 shows the transfer functions for the Linnecar's exponential electrode with $a = 2.63$ and $l = 190$ mm. We can find that the notches appearing in the red line (rectangle electrode) diminish in the blue line, while Linnecar's exponential electrode theoretically keeps oscillating at high frequency as

$$F(\omega) \sim \frac{k_0}{2}(1 - e^{-a - i\frac{2\omega l}{c}}). \quad (5)$$

As Eq.(1) shows, the transfer function $F(\omega)$ can be interpreted as the Fourier transform of the step function, which

ISBN 978-3-95450-178-6

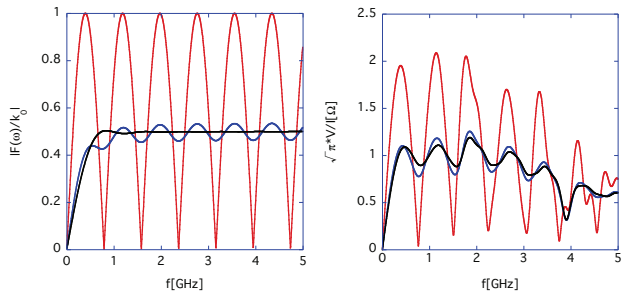

Figure 2: The theoretical (left) and the simulation (right) results of the transfer function $|F(\omega)|$.

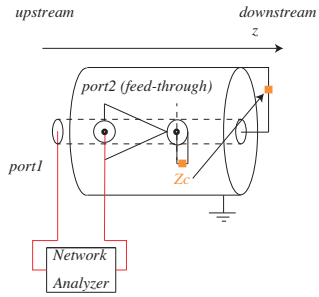

Figure 3: A schematic of the setup for the measurement of the transfer function.

exists only between zero to l, where the coupling function $k(z)$ plays a window function role [3]. From a mathematical point of view, the optimization of the electrode shapes is simplified to the issue how to choose the window function. Finally, we find that a polynomial function [4] :

$$k(z) = k_0 \frac{(l-z)^\sigma}{l^\sigma}, \tag{6}$$

with $\sigma = 2.63$, is the best choice for the purpose. The transfer function is given by

$$F(\omega) = -\frac{k_0}{2} \frac{e^{-i\frac{2\omega l}{c}}(\Gamma[1+\sigma] - \Gamma[1+\sigma, -i\frac{2\omega l}{c}])}{(-i\frac{2\omega l}{c})^\sigma}, \tag{7}$$

where $\Gamma(z)$ and $\Gamma(a,z)$ are the Γ- and the incomplete Γ-functions, respectively. Contrary to the exponential case, the formula approximated by

$$F(\omega) \sim \frac{k_0}{2}(1 - \frac{e^{i(\frac{\pi\sigma}{2} - \frac{2\omega l}{c})}\Gamma[1+\sigma]}{(\frac{2\omega l}{c})^\sigma}), \tag{8}$$

damps and approaches $k_0/2$ at high frequency. Overall behavior of the result is shown in the black line in the left figure of Fig.2. The frequency characteristic of the transfer function becomes much flatter for the polynomial function.

The simulation is performed by CST Studio [5]. In this simulation, four electrodes are placed 90 degree apart in the chamber with $a_1 = 65$ mm radius and 5 mm thickness. The respective electrodes are sophisticatedly reclined in order that Z_c of the electrode preserves 50 Ω along the electrode. In the simulations, the transfer function is obtained by dividing the Fourier transform of the beam-induced voltage at the upstream port by that of the beam current. The blue, the red and the black lines in the right figure of Fig.2 show the results for the exponential, the rectangular and the polynomial electrodes, respectively. As theoretically expected, the amplitude fluctuation is most suppressed in the polynomial results.

The transfer function $F(\omega)$ is obtained by the measurement of S_{21} in the setup shown in Fig.3. The downstream side of the chamber is terminated with the matched resistor. One port of the Network Analyzer (NA) is connected to the port at the entrance of the chamber, while the other port is connected to the wider end of the electrode.

In J-PARC MR [6], exponential electrodes with $l = 306$ mm are used for the intra-bunch feed-back system. Since it was difficult to bend them exponentially as required for a good impedance matching, we kept them straight as a flat plate.

The left figure of Fig.4 shows the measurement results of S_{21} for the exponential electrode. While the peak to peak modulation is about 30 % below 1 GHz, it is drastically worsen at high frequency. The right figure of Fig.4 shows the simulation results with $l = 280$ mm. The blue line shows the case that the electrode is put straight as a flat plate, while the red line shows the one that the electrode is precisely reclined to preserve Z_c. The peak to peak modulation on the blue line is worsen to about 30 % below 1 GHz, apart from about 23 % on the red line.

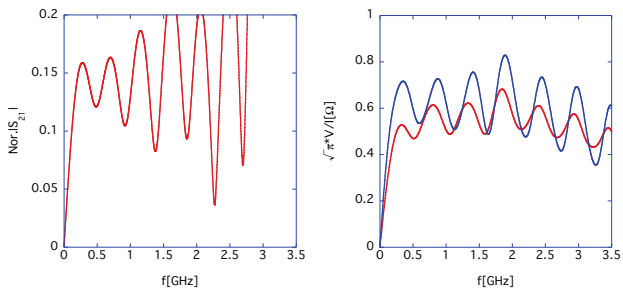

Figure 4: Measured S_{21} (left) for the exponential electrode, and simulation results (right).

From these results, the precise bent of the electrode is a key issue to make maximum use of the merit of electrode shapes, which is quite difficult in practice. Consequently, we start with a simple shape and gradually increase its complexity to improve the frequency performance.

THE TRANSFER FUNCTION OF ELECTRODES TAPERED BY LINEAR FUNCTIONS

The simplest shape next to the rectangle electrode is a triangle. It requires no sophisticatedly bending to attain a good impedance matching.

The coupling function of the triangle electrode is given

ISBN 978-3-95450-178-6

by [7]

$$k_{triangle}(z) = k_0 \frac{(l-z)}{l}. \quad (9)$$

Accordingly, the transfer function is calculated as

$$F(\omega) = \frac{k_0}{2} \frac{i(1 - i\frac{2\omega l}{c} - e^{-i\frac{2\omega l}{c}})}{\frac{2\omega l}{c}}. \quad (10)$$

The red line in the left figure of Fig.5 shows the theoretical result of the triangle electrode with $l = 280$ mm. The blue line shows the result for the exponential one, for reference. Except the large overshoot at low frequency, the triangle electrode has a better frequency characteristic compared with that for the exponential electrode.

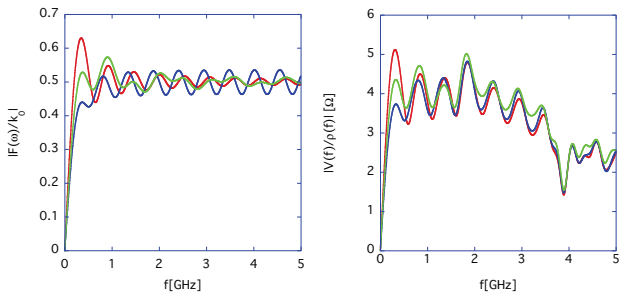

Figure 5: The theoretical (left) and the simulation (right) results of the transfer functions.

By introducing one more complexity in the shape, this overshoot effect can be mitigated. Let us replace the long, straight sides of the triangle by a three-point polyline. This deformation transforms the triangle to a concave pentagon. The concave pentagon electrode needs to be bent only once at the middle point of the polylines for a good impedance matching. Thus, its fabrication and setup remain to be easy.

The coupling function is given by

$$k_{pentagon}(z) = \begin{cases} k_0(1 - \frac{(1-y_0)z}{x_0}), \text{for } z \le x_0, \\ -k_0 \frac{y_0(z-l)}{(l-x_0)}, \text{for } z > x_0, \end{cases} \quad (11)$$

where x_0 and y_0 specify a middle point location. Theoretically, the optimal position of the middle point provides

$$x_0 = \frac{8.5}{20} l, y_0 = \frac{7.5}{20}. \quad (12)$$

The theoretical transfer function of the concave pentagon electrode is shown by the green line in the left figure of Fig.5. The simulation results for all shapes of electrode are shown in the right figure of Fig.5. The overshooting effect in the triangle electrode is suppressed in the concave pentagon electrode. Moreover, the frequency characteristic of the concave pentagon (green) is surprisingly similar to that of the exponential electrode (blue).

WORKING OF THE APRON PLATES

The signal strength in the simulation result (the right figure of Fig.5) starts to be declined beyond the first transverse magnetic (TM) waveguide mode:

$$f_c = \frac{0.114}{a_1(= 65\text{mm})} (\simeq 1.76\text{GHz}). \quad (13)$$

This is due to a large gap between the chamber wall and the upstream end of the electrode. Some of the image current running on the chamber surface before the electrode jump to the electrode over this gap as a displacement current. For short wavelength modes, this gap prevents a smooth flow of the displacement current and thus the image current running on the electrode loses some parts of high frequency components.

By attaching a plate perpendicular to the upstream edge of the plate (See the left picture of Fig.6. From hereon, we call this plate "an apron".), this gap for the image current can be reduced. The right figure of Fig.6 shows the simulation results with the apron for the triangle (red) electrode, the exponential one (blue) and the concave pentagon one (green). Comparing that with the right figure in Fig.5, we find that the signal strength is maintained up to the second TM mode :

$$f_c = \frac{0.262}{a_1} (\simeq 4\text{GHz for } a_1 = 65 \text{ mm}). \quad (14)$$

The apron plate is effective to sustain a signal strength up to higher frequency as a chamber has a smaller radius [7].

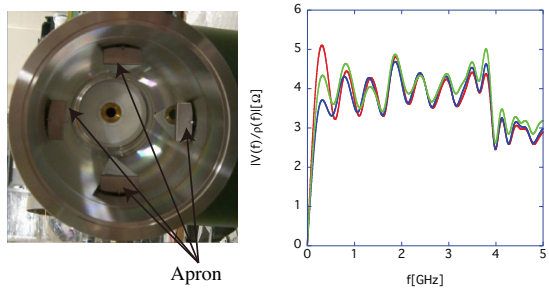

Figure 6: A photo of the apron on the triangle electrodes (left), and the simulation results (right) for $l = 280$ mm.

MEASUREMENTS OF THE TRANSFER FUNCTIONS

Measurements are done by preparing for four types of electrodes (the triangle and the concave pentagon electrodes with and without the apron.). A schematic picture of the setup is shown in Fig.3. The inner conductor is installed in the chambers with 134 ϕ, where the 306 mm long four electrodes are housed. The inner conductor and the chambers make a coaxial structure with $Z_c = 50\ \Omega$. The chamber is sandwiched between two conical tapered coaxial section to suppress reflection effects while keeping a constant 50 Ω characteristic impedance for the NA operation.

The transmission coefficient S_{21} is measured with 4-port Agilent Technologies ENA Series E5071C. The calibration is done by 2-port electric calibration module 85092b [8].

ISBN 978-3-95450-178-6

The measurement results are shown in Fig.7. The red and the green lines show the results for the triangle and the concave electrodes, respectively. The left and the right figures show the results without and with the apron, respectively. The overshooting effect appearing in the red lines diminishes in the green lines. As the right figure shows, the apron is effective to suppress the signal fluctuations.

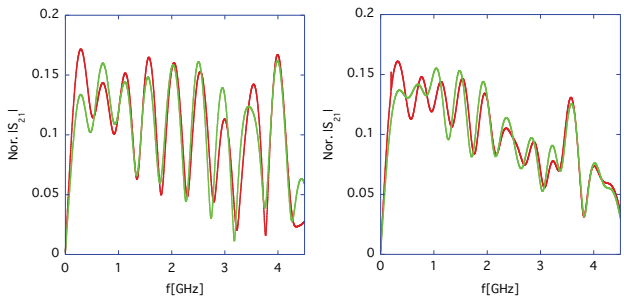

Figure 7: Measured S_{21} without (left) and with (right) the apron.

We measured the impedance distribution along the electrode by time domain reflectometry method, where the down stream port on the electrodes are terminated by 50 Ω resistor, and the upstream port is connected to a Tektronix DSA8200 Sampling Oscilloscope [9]. The measurement results for the triangle (left) and the concave pentagon(right) electrodes are shown in Fig.8. To the goal of the excellent impedance matching, more significant efforts are worthy to be made in the fabrication process. We expect that the gradual decline of the signal strength in the right figure of Fig.7 will be recovered by improving the impedance mismatch along the electrodes.

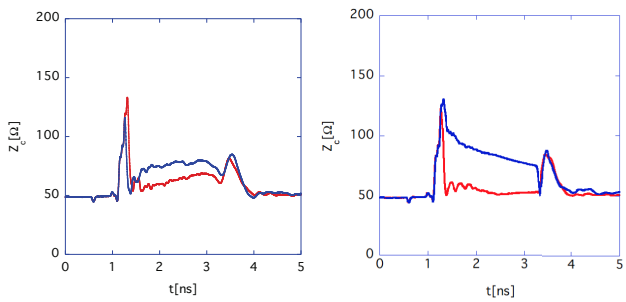

Figure 8: Measurement results of the impedance distribution along the triangle (left) and the concave pentagon (right) electrodes with (blue) and without (red) the apron.

IMPEDANCES OF THE ELECTRODES

Now, let us investigate the beam-coupling impedances of the electrodes. The longitudinal impedance Z_L is measured by connecting the second port of the NA to the exit of the chambers both housing the electrodes and housing no electrode (as a reference pipe). Both ends of all electrodes are terminated by the matched resistors.

The measured S_{21} are converted to Z_L by using the standard log-formula [10]:

$$Z_L = -2Z_c \log \frac{S_{21}}{S_{21}^{(ref)}}, \tag{15}$$

where S_{21} and $S_{21}^{(ref)}$ are the transmission coefficients for the device under test and for the reference pipe, respectively.

At first, we theoretically derive the formula of Z_L based on the transmission line model. We assume port 1 and 2 are located at $z = 0$ and $z = l$, respectively. Equations are given by

$$\frac{dV_1}{dz} = -i\omega L(z) I_1 - i\omega M(z) I_{inner}, \tag{16}$$

$$\frac{dI_1}{dz} = -i\omega \frac{L_{inner}}{c^2(L(z)L_{inner} - M(z)^2)} V_1 + i\omega \frac{M(z)}{c^2(L(z)L_{inner} - M^2(z))} V_{inner}, \tag{17}$$

$$\frac{dV_{inner}}{dz} = -i\omega L_{inner} I_{inner} - i\omega M(z) I_1, \tag{18}$$

$$\frac{dI_{inner}}{dz} = i\omega \frac{M(z)}{c^2(L(z)L_{inner} - M(z)^2)} V_1 - i\omega \frac{L(z)}{c^2(L(z)L_{inner} - M(z)^2)} V_{inner}, \tag{19}$$

where $L(z)$, V_1 and I_1 are the self-inductance, the voltage and the current of the electrode, respectively, L_{inner}, V_{inner} and I_{inner} are the self-inductance, the voltage and the current of the inner conductor, respectively, and $M(z)$ is the mutual inductance between the inner conductor and the electrode.

It is quite difficult to solve Eqs.(16)-(19) exactly. Let us make the approximations to solve them : the coupling between the inner conductor and the electrode is weak ($M^2 \ll LL_{inner}$), and regard M as a perturbation and solve them iteratively. Finally, the transmission coefficient S_{21} is approximately calculated, and Z_L is given by

$$Z_L = \frac{2n_{NE}\omega^2}{Z_c} \int_0^l dz'' \int_0^{z''} dz' M(z') M(z'') e^{i\frac{2\omega}{c}(z'-z'')}, \tag{20}$$

where n_{NE} the number of the electrodes in the chamber (In this description, the negative value of the imaginary part corresponds to be inductive impedances. For comparison with a simulation result, the sign is made opposite in the red dashed line of Fig.9).

For the exponential electrode, the mutual inductance is approximated as

$$M(z) \simeq \frac{Z_0}{2\pi c} \log[\frac{a_1}{a_1 - \Delta e^{-\frac{a}{l}z}}], \tag{21}$$

where Δ is the distance between the electrode and the chamber at $z = 0$. The difference of the electrode shapes

ISBN 978-3-95450-178-6

is confined in the z-dependence of the logarithmic function, by which we expect that the impedances do not significantly depend on the electrode shapes.

The theoretical (red) and the simulation (blue) results for the exponential electrode are shown in the left figure of Fig.9. The theoretical result shows that it is inductive, and that the wake function behaves like the δ'-function, as shown by the simulation result in the right figure.

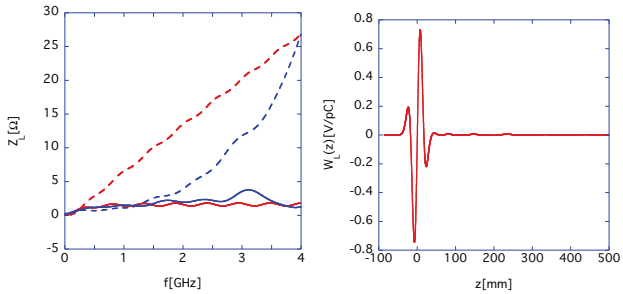

Figure 9: The theoretical (red) and the simulation (blue) results of Z_L (left) for the exponential electrode ($a = 2.63$, $l = 280$ mm), and the simulation result of the wake function (right). The solid and the dot lines show the real and the imaginary parts of the impedance.

Here, let us investigate the impedance dependence on the electrode shapes. The scaled picture of the simulation results below 1GHz are shown in Fig.10. The Z_L is shown in the upper figure. The Z_T are shown in the lower figure, as well. The left and the right figures show the results without and with the apron, respectively. The red, the blue and the green lines show the results for the triangle, the exponential and the concave pentagon electrodes, respectively. The amount of the value of the impedances for all shapes is the same order of magnitudes, as theoretically expected. Moreover, the simulation results suggest that the impedances do not strongly depend on the existence of the aprons.

The measurement results of Z_L are shown in Fig.11. The left and the right figures show the results without and with the apron, respectively. The impedances with the aprons are enhanced compared to those without the aprons within a factor or two, because the electrodes with the aprons are more apart from the chamber wall than those without them, violating impedance-matching (refer to Fig.8). Figure 10 suggests that this impedance enhancement should be reduced by improving the impedance-mismatch along the electrodes.

SUMMARY

The high frequency performance of the exponential electrode in J-PARC MR (Fig.4) can be improved by replacing it with the concave pentagon electrode with the apron (Fig.7). The apron plate on the wider end of the electrode helps to maintain the signal strength up to the second TM-mode. The merit of the concave pentagon with the apron is that, its fabrication is easier than that of the exponential

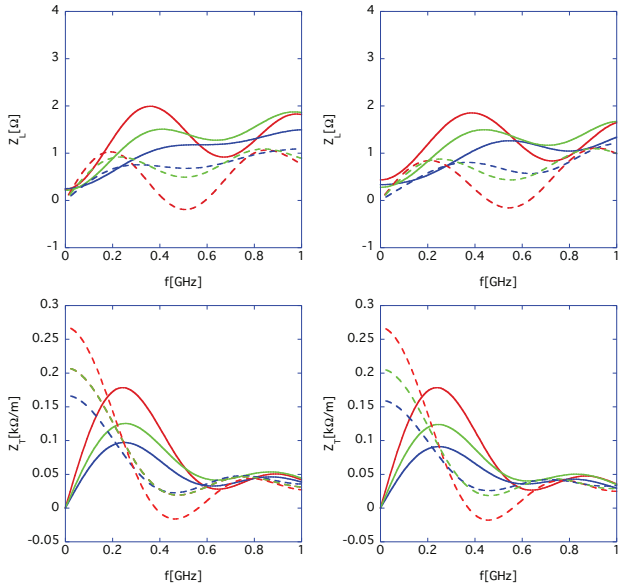

Figure 10: The simulation results of Z_L (upper) and Z_T (lower) without (left) and with (right) the apron. The solid and the dashed lines show the real and the imaginary parts of the impedances, respectively.

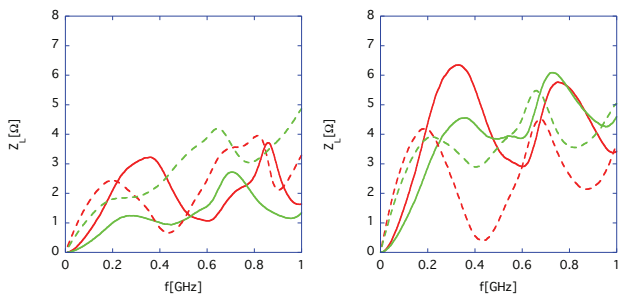

Figure 11: Measured Z_L for the triangle (red) and the concave (green) electrodes, respectively. The solid and the dashed lines show the real and the imaginary parts of the impedances, respectively.

electrode.

The simulation results suggest that the impedances do not significantly depend on the electrode shapes, and whether the aprons are attached on the electrodes. We expect that the significant efforts to improve the impedance-mismatch along the electrodes will realize the better frequency performance as well as the lower coupling impedances.

ACKNOWLEDGMENTS

This work was partially supported by MEXT KAKENHI Grant No. 25105002.

ISBN 978-3-95450-178-6

REFERENCES

[1] B. M. Oliver, Proc. I.R.E., Vol 42, No. 11, 1686, (1954)

[2] T. Linnecar, CERN-SPS-ARF-SPS/78/17, CERN, (1978)

[3] F. G. Harris, Proceedings of the IEEE, Vol. 66, 51, (1978).

[4] Y. Shobuda and Y. H. Chin, PRST AB 17, 092801, (2014)

[5] CST STUDIO SUITE, http://www.cst.com

[6] http://j-parc.jp/index-e.html

[7] Y. Shobuda *et al*, Phys. Rev. AB 19, 021003, (2016)

[8] *http* : *//www.home.agilent.com/*

[9] *http* : *//jp.tek.com/*

[10] *Handbook of Accelerator Physics and Engineering*, edt by A. Chao *et al*, (Singapore, World Scientific, 2013)

ISBN 978-3-95450-178-6